Concrete cover delamination model for non-uniform corrosion of reinforcements

Yanlong Zhang and Ray Kai Leung Su[1]
Department of Civil Engineering, The University of Hong Kong, Pokfulam Road, Hong Kong, PRC

Abstract: Cover delamination failure caused by the corrosion of closely spaced rebars is commonly found in deteriorated reinforced concrete (RC) structures. However, analytical studies carried out on this failure mode of RC structures are rare. In response, this paper proposes a novel analytical model for cover delamination which takes into account the interaction between the neighboring corroded rebars, non-uniform distribution of rust around the steel/concrete interface, and boundary conditions of the concrete surface. This simple model enables manual prediction of the bulging deformation of the cover surface and the maximum thickness of rust. The predicted results are then verified with numerically derived results from a nonlinear finite element analysis. Finally, the effects of the rebar spacing, tensile strength of concrete and cover thickness on the bulging of the concrete cover surface and the maximum thickness of rust are studied with the verified analytical model.

Keywords: Cover delamination; Non-uniform corrosion; Concrete cover; Durability; Analytical modeling

1. Introduction

Concrete cover cracking, spalling and delamination are all caused by rebar corrosion, which is one of the primary reasons for the deterioration of reinforced concrete (RC) structures [1, 4, 5] as the corrosion-induced damage causes loss of integrity in the concrete cover, and reduces the bond strength between the steel bars and concrete as well as the strength of the rebars. Consequently, the serviceability, strength, durability and ductility of RC structures are adversely affected [6-9]. The total cost for the maintenance and repair of corrosion-induced deterioration of RC structures worldwide has been estimated to be around USD100 billion each year [11].

It is important to investigate the cover damage caused by non-uniform rebar corrosion which can be commonly observed in practice. The reason of non-uniform distribution of rust is because the penetration of chloride/carbonation, moisture and oxygen into concrete is often not uniform around the perimeter of the rebars [12]. More rust is usually found on the side of the rebars that faces the cover surface [13-16] due to the macrocell corrosion of the rebars [17]. Previous studies have investigated cover failure caused by the non-uniform corrosion of rebars around the cross section of rebars [16, 18-25] and along the rebar themselves [25]. In this study, only non-uniform corrosion (not uniform) around the circular cross section of the rebars is

1 Corresponding author. Tel.:+852 2859 2648
E-mail address: klsu@hku.hk (RKL Su)

considered.

A number of studies in the existing literature have examined the corrosion-induced damage of concrete covers by modeling the covers as thick-walled cylinders [4, 6, 26-28]. However, these models cannot simulate flat concrete surfaces with multiple embedded rebars that are found in most RC components. The major shortcomings of using thick-walled cylinder models to simulate the corrosion induced cracking of concrete covers are summarized as follows. First, the confinement effect of concrete that surrounds the cover (thick-walled cylinder) is ignored but in actuality, can prolong the service life of RC structures [1, 29]. Despite that some studies [1, 29] have taken into consideration the effects of confinement in thick-walled cylinder models, the expansion pressure caused by the corrosion of the rebars was assumed to be uniformly distributed around the rebars. It is well known that the calculated effects of the pressure of corrosion and volume of rust on cover cracking that assume a uniform corrosion are not the same as using non-uniform corrosion [23, 30, 31]. Second, the effects of the rebar spacing and the interaction between the neighboring rebars that are corroded cannot be simulated by using a thick-walled cylinder model with a single rebar. Third, the different types of failure, such as cracking, spalling or delamination, cannot be examined separately by using a thick-walled cylinder model.

Cover surface cracking caused by the corrosion of a single rebar has also been extensively studied [4, 32-34]. However, if the proposed methods are applied to analyses of cover delamination due to multiple rebars, the results could be erroneous as the damage mode of these two types of cover failure are very different. Furthermore, previous results [12, 22, 35, 36] have shown that a large number of corroded rebars can lead to cover delamination prior to the cracking of the cover surface; see Fig. 1.

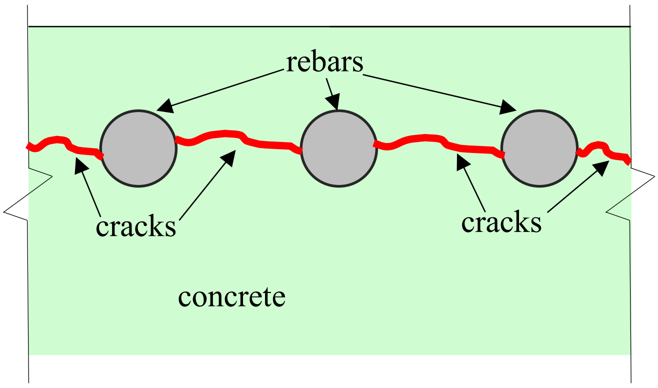

Fig. 1 Concrete cover delamination in RC beam

There is a paucity of work in the literature on corrosion-induced cover delamination [37]. While Li et al. [38] proposed an analytical model to predict the time to cover delamination due to corrosion of the steel reinforcements based on the crack opening in concrete, the model is based on a thick-walled cylinder and assumes that there is uniform corrosion of the rebars without taking into consideration the interaction between the neighboring corroded rebars. Sterritt [39] proposed a simple method to predict the time to cover delamination by taking into consideration the rust volume, corrosion rate and rebar diameter. However, Sterritt [39] did not consider rebar spacing which is a critical parameter that affects the progression of cover delamination [12]. Although the initiation of cracking and the width of cracks across the plane of the corroded rebars have been studied by using numerical models [22, 35, 40] or a numerical model along with an analytical method [12], it is still difficult to directly measure the internally connected cracks and numerical methods are relatively complex and difficult to be implemented by practicing engineers. Furthermore, the process and progression of cover delamination are still unclear. Hence, it is imperative to develop a simple analytical model to simulate the deterioration process of cover delamination and estimate the thickness of the rust.

In this study, a novel model is proposed to simulate cover delamination caused by the corrosion of closely spaced rebars in RC components by taking into consideration: (1) the interaction between the neighboring corroded rebars, (2) the non-uniform distribution of rust around the steel/concrete interface, and (3) a flat concrete surface. Furthermore, a finite element (FE) analysis will be carried out with ATENA to verify the proposed analytical model.

2. Proposed cover delamination model

In this section, a discussion will be provided on the development of a cover delamination model to simulate the process of cover delamination due to the non-uniform corrosion of closely spaced rebars. The term ‘closely spaced’ means that the rebar spacing/clear spacing between the rebars is sufficiently close enough so that both the internally connected cracks across the plane of the corroded rebars and the bulging of the concrete cover surface caused by the corrosion of rebars could be affected by the neighboring corroded rebars. Based on the results obtained from the FE model which will be discussed in Section 3, the entire process of the bulging of the concrete cover surface can be observed as three stages: (1) the elastic stage of the concrete, (2) partial cracking stage and (3) the stage in which there is development of delamination in the concrete cover.

2.1 Distribution of rust

In this study, the delamination of the concrete cover is analyzed as a two dimensional problem for simplicity and computational efficiency. However, the shape of the distribution of the rust around a rebar is beyond the investigation scope of this study. Therefore, the distribution of the rust is assumed to be in a crescent shape [13, 16, 23], as illustrated in Fig. 2. In the figure, D is the rebar diameter, $d_{s,max}$ is the maximum thickness of the corroded steel and $d_{r,max}$ is the maximum thickness of the rust. The volume of the corroded steel V_{steel}, can be obtained by using:

$$V_{\text{steel}} = \frac{1}{2}\frac{\pi D^2}{4} - \frac{1}{2}\frac{\pi D}{2}\left(\frac{D}{2} - d_{\text{s,max}}\right) = \frac{\pi D d_{\text{s,max}}}{4} \tag{1}$$

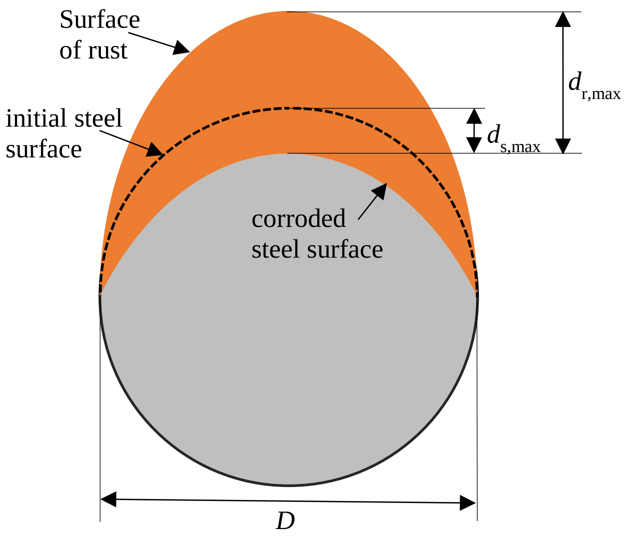

Fig. 2 Crescent shaped distribution of rust

2.2 Properties of materials

When a linear elastic stress-strain relationship is assumed for concrete in tension, then

$$\varepsilon_{\text{t}} = \frac{\sigma_{\text{t}}}{E_{\text{c,ef}}} \tag{2}$$

where ε_t is the tensile strain of concrete, σ_t is the tensile stress and $E_{c,ef}$ is the effective elastic modulus of concrete which can be expressed as:

$$E_{\text{c,ef}} = E_{\text{c}}/(1 + \phi_{\text{ct}}) \tag{3}$$

where E_c is the elastic modulus of concrete and ϕ_{ct} is the creep coefficient of concrete.

Once the tensile stress reaches the tensile strength of the concrete, the corresponding strain of the concrete ε_{ct} can be expressed as:

$$\varepsilon_{\text{ct}} = \frac{f_{\text{t}}}{E_{\text{c,ef}}} \tag{4}$$

where f_t is the tensile strength of the concrete.

Cracking initiates after the concrete reaches tensile strength. In this study, the fictitious crack opening $w(x)$ is assumed to be linearly proportional to the coordinate x

along the fracture process zone (FPZ) with the origin at the crack tip. The relationship between w(x) and x can be expressed as:

$$w(x) = \frac{x}{L_{\mathrm{FPZ}}} w_{\mathrm{c}} \tag{5}$$

where w_c is the crack tip opening displacement which corresponds to zero residual tensile stress on the crack surface and L_{PFZ} is the length of the FPZ.

As the Young's modulus of steel (~200 GPa) is much higher than that of concrete (about 20-30 GPa), the elastic deformation of rebars can be neglected [27] and therefore, the rebars are treated as rigid bodies in this analysis. Furthermore, when the Young's modulus of the rust E_{rust} or the bulk modulus of the rust K_{rust} (which is defined as the ratio of the infinitesimal pressure increase to the resulting relative decrease in the volume, and can be expressed as $K_{rust} = E_{rust}/3/(1\text{-}2v_{rust})$ where v_{rust} is the Poisson's ratio of rust) is high enough, for instance, $E_{rust} \geq 500$ MPa [1], $E_{rust} \geq 1$ GPa [27], $K_{rust} \geq 300$ MPa [41] or $K_{rust} \geq 4$ GPa [42], the effect of the deformation due to rust on calculating the volume of rust can also be neglected [1, 27, 41, 42]. For simplicity, rust is considered to be a rigid body in this study.

2.3 Process and progression of cover delamination

Fig. 3 shows the progression of the bulging of the concrete cover surface of an RC member with a flat surface due to delamination. The RC member which has multiple rebars is illustrated in Fig. 3a in which c is the cover thickness and S_b denotes the rebar spacing. In this figure, a corroded interior rebar together with the exterior part of the concrete with a width of S_b shown inside the dashed box will be elaborated in the subsequent sections to simulate the cover delamination process.

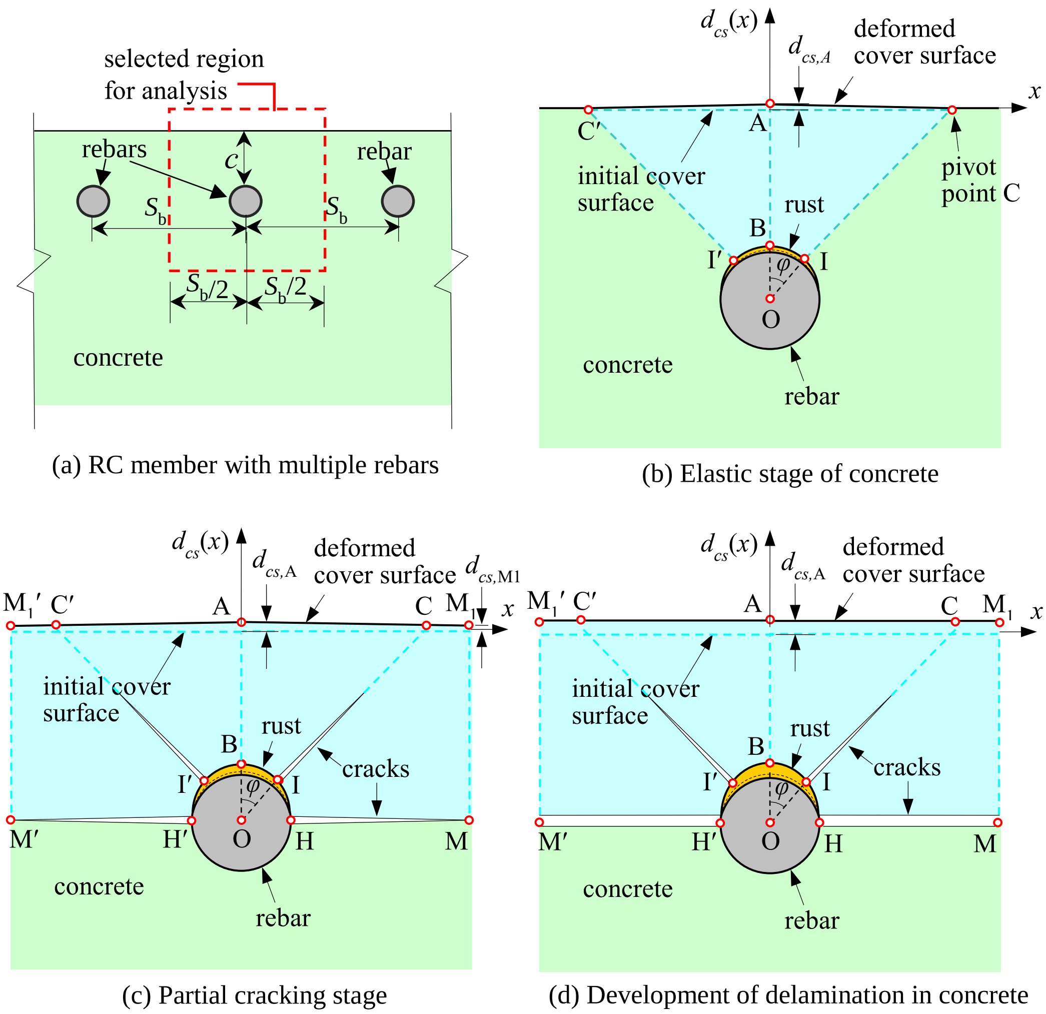

Fig. 3 Crack initiation to cover delamination

After the porous zone around the rebar is covered with rust, the process of the bulging of the concrete cover surface can be observed as three stages: (1) the elastic stage of the concrete, (2) partial cracking stage and (3) the stage in which there is development of delamination in the concrete cover.

The elastic stage of the concrete (see Fig. 3b) is initiated with rust induced expansion pressure onto the surrounding concrete and ends when cracking starts around the steel/concrete interface. Here, the initiation of cracking is defined as the point when the tensile stress of the concrete reaches the tensile strength of the concrete f_t. As the concrete cover remains elastic, this stage is called the elastic stage of the concrete. Due to the elastic shortening of the concrete, the maximum amount of bulging of the concrete cover surface along the vertical line of symmetry at Point A, $d_{cs,A}$, is slightly less than the net maximum thickness of the rust $d_{f,max}$ at Point B (which is defined as the maximum thickness of rust that induces expansion pressure onto the surrounding concrete). Furthermore, the corrosion-induced expansion pressure on the side near the concrete cover pushes against the concrete cover and causes the elastic concrete parts ABIC and ABI′C′ to rotate about the pivot points (Points C and C′) as shown in Fig. 3b, in which Points B, I and I′ are all found at the steel/concrete interface. In this stage, the deformation of the concrete cover surface is mainly from the rotation of the concrete cover. It can be assumed that the surface deformation along AC, $d_{cs}(x)$, decreases linearly from $d_{cs,A}$ to 0 as shown in Fig. 3b.

The second stage of the bulging which is called the partial cracking stage is illustrated in Fig. 3c. The figure shows that Points H and H′ are at the steel/concrete interface and Points M and M′ and Points M_1 and M_1' are on the plane of the rebars and on the cover surface, respectively. This stage starts with the initiation of cracks at the steel/concrete interface and ends with the initiation of cover delamination which is defined as the moment when there is no tensile capacity along HM, which is the delamination plane. During this stage, cracks gradually penetrate along HM which results in internally connected cracks on the plane of the corroded rebars. The width of the internal cracks progressively increases with the increase of rust thickness. With the initiation of cover delamination, the cracks along HM become wide enough so that the concrete can no longer provide resistance against the residual tensile stress, which leads to uplifting movement of the concrete part $ABHMM_1$. Thus, the deformation due to a bulging surface $d_{cs}(x)$ is a constant and equal to $d_{f,max}$. Hence, in the partial cracking stage, the deformation of the concrete cover surface is determined by both (1) the rotation of the concrete part ABIC which is mainly caused by the confinement effect of the concrete along the delamination plane HM and (2) the vertical movement of $ABHMM_1$ which is caused by cracking along HM. Together, they lead to less bulging of the concrete cover surface that is approximately linear from Points A to M_1 (see Fig. 3c). Furthermore, the effect of the rotation of ABIC is reduced with crack growth, while the uplifting movement of $ABHMM_1$ gradually increases.

The third stage is the development of delamination in the concrete cover. In this stage, the uplifting movement of the concrete cover is the main reason for the deformation of the concrete cover surface and $d_{f,max}$ is equal to the bulging along AM_1 as shown in Fig. 3d.

2.4 Corrosion induced expansion

During the progression of steel corrosion, four sources contribute to the total volume of rust, V_{rust}, [1, 6, 43]: (1) the volume of rust in the corroded steel itself, V_{steel}; (2) the volume of rust in the porous zone at the steel/concrete interface, V_{porous}, (3) the net amount of rust that induces expansion pressure onto the surrounding concrete, V_{net}, and (4) the amount of rust that penetrates into the corrosion-induced cracks, V_{cracks}. Therefore, the total volume of rust can be calculated as:

$$V_{\text{rust}} = V_{\text{steel}} + V_{\text{porous}} + V_{\text{net}} + V_{\text{cracks}} \tag{6}$$

As all of the rust is produced from the corrosion of steel, the total volume of rust can also be expressed as:

$$V_{\text{rust}} = \beta V_{\text{steel}} \tag{7}$$

where β is the ratio of the volume of rust to that of the original corroded steel. Therefore, the relationship between $d_{s,max}$ and $d_{r,max}$ can be obtained as follows:

$$d_{\text{r,max}} = \beta d_{\text{s,max}} \tag{8}$$

For each component of rust, the parameter β varies from 1.7 to 6.15, like FeO = 1.7, Fe_2O_3 = 2.1, Fe_3O_4 = 2, α-FeO(OH) = 2.95, β-FeO(OH) = 3.53, γ-FeO(OH) = 3.07, $Fe(OH)_2$ = 3.6, $Fe(OH)_3$ = 4.0, $Fe(OH)_3 3H_2O$ = 6.15 [4, 44], while in practice, the rust is a mixture with different components, and β for the mixture is experimentally determined as around 3 by the Sanz et al. [45].

The porous zone around the steel/concrete interface can accommodate some rust and therefore, prolong the period of deterioration of the concrete cover [1, 4, 26, 46]. In this study, it is assumed that rust can only migrate into the concrete area that is adjacent to the corroded steel in non-uniform corrosion [19]. Therefore, the volume of rust that penetrates into the porous zone around the corroded steel can be calculated as:

$$V_{\text{porous}} = \frac{\pi d_0}{2}(D + d_0) \tag{9}$$

where d_0 is the thickness of the porous zone.

Although rust can penetrate into the surrounding concrete and damage the concrete cover at the same time [43, 47, 48], it is assumed here for simplicity that rust migrates into the porous zone first and then expansion pressure develops and is exerted onto the surrounding concrete [4, 27]. Previous studies suggest that the thickness of the porous zone is between 12.5 μm ≤ d_0 ≤ 120 μm [4, 26, 27, 49], and its thickness is mainly affected by the steel rebar (including geometry, orientation, surface state at the time of concrete casting), concrete properties (including mix proportions, hardening, curing, execution, ageing), and entrapped/entrained air voids [46].

As there is no consensus on whether rust penetrates into corrosion-induced cracks (and if so, how much) [25, 43, 50-52], the volume of the rust in the cracks is considered to be 0, i.e. V_{cracks} = 0, in this study.

The maximum thickness of the corroded steel that produces the rust that migrates into the porous zone, $d_{s,0,max}$, can be obtained by inserting Eqs. (1), (7) and (9) into Eq. (6), as follows:

$$d_{\text{s,0,max}} = \frac{2d_0}{\beta - 1} \tag{10}$$

Once the porous zone is filled with rust, the net maximum thickness of the rust $d_{\mathrm{f,max}}$ that induces expansion pressure onto the surrounding concrete can be expressed as:

$$d_{\mathrm{f,max}} = (\beta - 1)\left(d_{\mathrm{s,max}} - d_{\mathrm{s,0,max}}\right) \tag{11}$$

2.5 Elastic stage of concrete

In this stage, the concrete cover is elastic and has no cracks. Therefore, a linear elastic process can be used to analyze the concrete cover deformation. The concrete cover can be considered as an elastic thick-walled cylinder with an inner diameter of $D/2$ and outer diameter of $D/2 + c$. Therefore, the bulging of the concrete cover at Point A, $d_{\mathrm{cs,A}}$, can be calculated as [53]:

$$d_{\mathrm{cs,A}} = \frac{2d_{\mathrm{f,max}}D(D+2c)}{D^2(1-v)+(1+v)(D+2c)^2} \tag{12}$$

where v is the Poisson's ratio of the concrete.

Fig. 3b shows the concrete parts ABIC and ABI′C′ which are assumed to be symmetrical around Line AB. Point O is the center of the non-corroded rebar and Points O, I and C are collinear. The distance between Points A and C, L_{AC}, is

$$L_{\mathrm{AC}} = \left(\frac{D}{2} + c\right)\tan\varphi \tag{13}$$

where φ is the angle of a diagonal crack, which typically varies between 40° and 65° [12, 20-22, 24, 30, 31].

During this stage, the deformation along AC decreases linearly from $d_{\mathrm{cs,A}}$ to 0. Therefore, when $S_{\mathrm{b}} \le 2L_{\mathrm{AC}}$ as shown in Fig. 4a, the bulging $d_{\mathrm{cs}}(x)$ can be calculated as:

$$d_{\mathrm{cs}}(x) = \frac{L_{\mathrm{AC}}-x}{L_{\mathrm{AC}}} d_{\mathrm{cs,A}} \;\; (0 \le x \le S_{\mathrm{b}}/2) \tag{14}$$

When $2L_{\mathrm{AC}} < S_{\mathrm{b}}$ as shown in Fig. 4b, $d_{\mathrm{cs}}(x)$ can be expressed as:

$$d_{\mathrm{cs}}(x) = \begin{cases} \frac{L_{\mathrm{AC}}-x}{L_{\mathrm{AC}}} W_{\mathrm{A,v,E}} & 0 \le x \le L_{\mathrm{AC}} \\ 0 & L_{\mathrm{AC}} \le x \le S_{\mathrm{b}}/2 \end{cases} \tag{15}$$

where x is the horizontal coordinate with Point A as the origin.

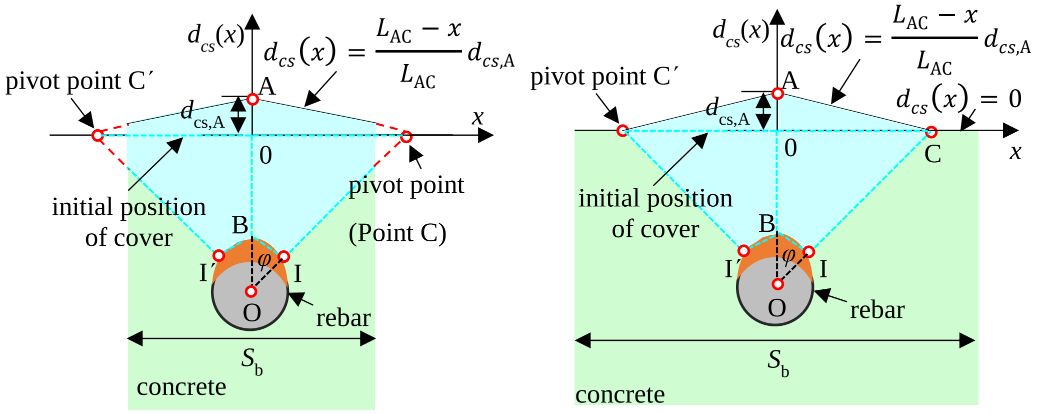

(a) Elastic stage of concrete when $S_b \leq 2L_{AC}$ (b) Elastic stage of concrete when $S_b > 2L_{AC}$

Fig. 4 Bulging of concrete cover surface in elastic stage of concrete

As the corrosion of the rebar advances, the concrete around the steel-concrete interface will stretch due to the expansion of rust. The elongation of concrete W_E can be calculated as follows:

$$W_E = \frac{\pi}{2}\left[\frac{3(D+d_{f,max})}{2} - \sqrt{\frac{D}{2}\left(\frac{D}{2} + d_{f,max}\right)}\right] - \frac{\pi D}{2} \tag{16}$$

In this stage, the tangential strain of the concrete around the corroded rebar at the steel/concrete interface is usually considered uniform [6, 26-28, 54]. Cracks initiate around the corroded rebar when W_E reaches the critical tensile deformation rate of the concrete W_{Ec}, i.e.,

$$W_E = W_{Ec} = \frac{\pi D \varepsilon_{ct}}{2} \tag{17}$$

When cracks initiate around the steel-concrete interface, the corresponding net maximum thickness of the corroded steel $d_{f,max,Ec}$ and the corresponding bulging of the concrete cover $d_{cs,Ac}$ at Point A can be obtained from Eqs. (16) - (17) and Eq. (12), respectively.

2.6 Partial cracking stage

After cracking takes place at the steel/concrete interface, the cracks gradually propagate beyond the interface as shown in Fig. 3c. During this stage, the bulging of the concrete cover surface is determined by both the rotation of ABIC and the uplifting movement of $ABHMM_1$. The proportion of the deformation, ρ, caused by the uplifting movement of $ABHMM_1$ is calculated as:

$$\rho = \frac{d_{f,max} - d_{f,max,Ec}}{d_{f,max,u} - d_{f,max,Ec}} \tag{18}$$

where $d_{f,max,u}$ is the net maximum thickness of the rust when the cover delamination is initiated which will be elaborated in Section 2.7.

Hence, $d_{\mathrm{cs,A}}$ consists of two parts: (1) $(1-\rho)d_{\mathrm{f,max}}$ which can be obtained from the elastic process as shown in Section 2.5, and (2) $\rho d_{\mathrm{f,max}}$ which can be obtained from the uplifting movement of the concrete cover. Thus, $d_{\mathrm{cs,A}}$ can be expressed as:

$$d_{\mathrm{cs,A}} = \frac{2d_{\mathrm{f,max}}D(D+2c)(1-\rho)}{D^2(1-\upsilon)+(1+\upsilon)(D+2c)^2} + \rho d_{\mathrm{f,max}} \tag{19}$$

Similarly, the bulging of the concrete cover surface at Point M_1 can be $\rho d_{\mathrm{f,max}}$ and therefore, the bulging along AC decreases linearly from $d_{\mathrm{cs,A}}$ to $\rho d_{\mathrm{f,max}}$. Hence, when $S_{\mathrm{b}} < 2L_{\mathrm{AC}}$ as shown in Fig. 5a, the bulging of the concrete cover surface along AC, $d_{\mathrm{cs}}(x)$, can be expressed as:

$$d_{\mathrm{cs}}(x) = \frac{2d_{\mathrm{f,max}}D(D+2c)(1-\rho)(L_{\mathrm{AC}}-x)}{L_{\mathrm{AC}}[D^2(1-\upsilon)+(1+\upsilon)(D+2c)^2]} + \rho d_{\mathrm{f,max}} \tag{20}$$

When $2L_{\mathrm{AC}} < S_{\mathrm{b}}$ as shown in Fig. 5b, $d_{\mathrm{cs}}(x)$ can be expressed as:

$$d_{\mathrm{cs}}(x) = \begin{cases} \frac{2d_{\mathrm{f,max}}D(D+2c)(1-\rho)(L_{\mathrm{AC}}-x)}{L_{\mathrm{AC}}[D^2(1-\upsilon)+(1+\upsilon)(D+2c)^2]} + \rho d_{\mathrm{f,max}} & 0 \le x \le L_{\mathrm{AC}} \\ \rho d_{\mathrm{f,max}} & L_{\mathrm{AC}} \le x \le S_{\mathrm{b}}/2 \end{cases} \tag{21}$$

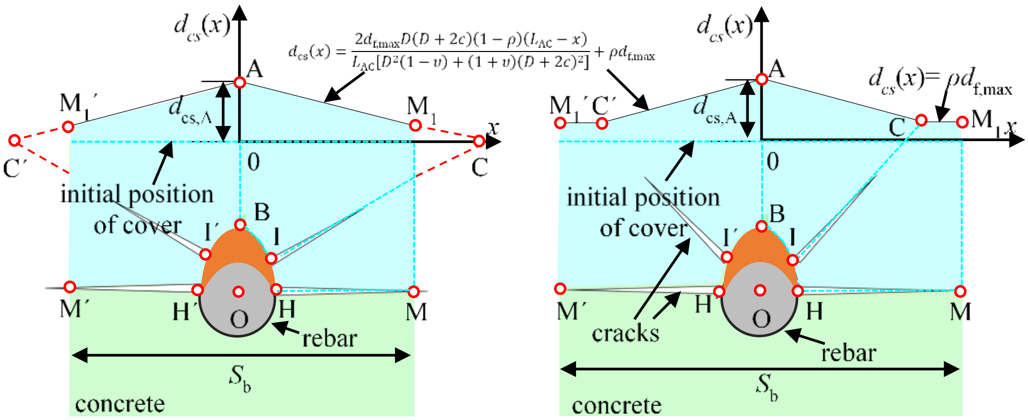

(a) Partial cracking stage when $S_{\mathrm{b}} \le 2L_{\mathrm{AC}}$ (c) Partial cracking stage when $S_{\mathrm{b}} > 2L_{\mathrm{AC}}$

Fig. 5 Bulging of concrete cover surface in partial cracking stage

2.7 Initiation of cover delamination

Once the crack tips of two neighboring rebars join together, the cracks penetrate through the plane of the two rebars and cause delamination of the concrete cover. Then, $d_{\mathrm{cs}}(x)$ is equal to the net maximum thickness of the rust, $d_{\mathrm{f,max,u}}$, i.e.,

$$d_{\mathrm{cs}}(x) = d_{\mathrm{f,max,u}} = d_{\mathrm{cs,A,u}} \tag{22}$$

where $d_{\mathrm{cs,A,u}}$ is the bulging of the concrete cover at Point A when the delamination of the cover starts.

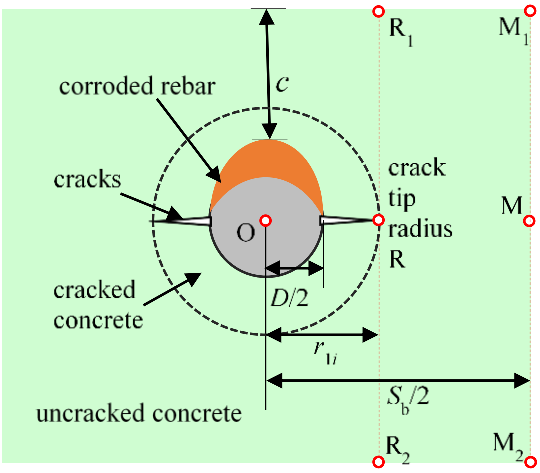

Fig. 6 Crack propagation caused by one single rebar

To obtain $d_{\mathrm{f,max,u}}$, the neighboring corroded rebars are examined separately. When a crack tip reaches Point R due to the corrosion of one of the rebars as shown in Fig. 6, the stress and strain of the concrete at the crack tip in the direction perpendicular to the crack is the tensile strength of the concrete f_{t}, and the corresponding critical tensile strain of the concrete $\varepsilon_{\mathrm{ct}}$. The partially cracked concrete cover with one rebar can be simulated as an elastic thick-walled cylinder with an inner diameter of r_{1i} and outer diameter of $S_{\mathrm{b}}/2$ as shown in Fig. 6. Therefore, based on the elastic process, the ratio of the vertical stress at Point R (f_{t}) to that at Point M ($\sigma_{\theta\mathrm{M}}$) can be expressed as [53]:

$$\frac{f_{\mathrm{t}}}{\sigma_{\theta\mathrm{M}}} = \frac{r_{1i}^2 + (S_{\mathrm{b}}/2)^2}{2r_{1i}^2} \tag{23}$$

In Fig. 6, the length of RR_1 is equal to that of RR_2 and the length of MM_1 is equal to that of MM_2. As there is no external load on the cover surface, the tensile strain of concrete is zero in the direction perpendicular to the cover surface (at Points R_1 and M_1). It is assumed that the tensile strain of concrete decreases linearly from the cracked surface (along RM) to the cover surface (along R_1M_1) and that the variation in the tensile strain of concrete on the two sides of the cracking (concrete parts RR_1M_1M and RR_2M_2M) are the same. Therefore, the deformation of the concrete at Point R, $W_{\mathrm{x,Ec}}$, can be calculated with:

$$W_{x,\mathrm{Ec}} = \varepsilon_{\mathrm{ct}}\left(c + \frac{D}{2}\right) \tag{24}$$

and the deformation of the concrete at Point M, $W_{\mathrm{M,Ec,}1i}$, can be determined by using:

$$W_{\mathrm{M,E,}1i} = \varepsilon_{\mathrm{M,E,}1i}\left(c + \frac{D}{2}\right) \tag{25}$$

where $\varepsilon_{\mathrm{M,E,}1i}$ is the strain of the concrete at Point M in the direction perpendicular to the crack and can be determined with:

$$\varepsilon_{\mathrm{M,E,}1i} = \frac{\sigma_{\theta\mathrm{M}}}{E_{\mathrm{c,ef}}} \tag{26}$$

The deformation of the concrete at Point M can be obtained by inserting Eqs. (4), (23), (24) and (26) into Eq. (25),

$$W_{\mathrm{M,E,1}i} = \frac{2r_{1i}^2 W_{x,\mathrm{Ec}}}{r_{1i}^2+(S_\mathrm{b}/2)^2} \tag{27}$$

During the partial cracking stage, the length of the FPZ is $r_{1i} - D/2$. Based on the assumption provided in Section 2.2 on the relationship between the crack opening and the length of the FPZ, the crack opening at Point H, $\mathrm{CMOD}_{\mathrm{H},1i}$, can be calculated as:

$$\mathrm{CMOD}_{\mathrm{H},1i} = \frac{r_{1\mathrm{i}}-D/2}{L_\mathrm{FPZ}} w_\mathrm{c} \tag{28}$$

Considering the interaction of the neighboring corroded rebars, the total deformation of the concrete at Point M, $W_{\mathrm{M,Ec},i}$, is equally affected by the two neighboring rebars. Therefore, $W_{\mathrm{M,Ec},i}$ can be expressed as:

$$W_{\mathrm{M,E},i} = 2W_{\mathrm{M,E,1}i} = \frac{4r_{1i}^2 W_{x,\mathrm{Ec}}}{r_{1i}^2+(S_\mathrm{b}/2)^2} \tag{29}$$

If the influence of the neighboring rebars on the crack opening at the steel surface (Point H) is neglected, the crack opening at that point due to the corrosion of multiple rebars can be determined by using:

$$\mathrm{CMOD}_{\mathrm{H},i} = \mathrm{CMOD}_{\mathrm{H},1i} = \frac{r_{1\mathrm{i}}-D/2}{L_\mathrm{FPZ}} w_\mathrm{c} \tag{30}$$

When $W_{\mathrm{M,E},i} = W_{x,\mathrm{Ec}}$, the delamination of the cover is initiated, and the critical crack tip radius $r_{1\mathrm{c}}$ can be obtained by combining Eqs. (24) and (29):

$$r_{1\mathrm{c}} = \frac{S_\mathrm{b}}{2\sqrt{3}} \tag{31}$$

Taking into consideration the elastic deformation of the concrete, $d_{\mathrm{f,max,u}}$ can be obtained by combining Eqs. (30) and (31):

$$d_{\mathrm{f,max,u}} = \frac{S_\mathrm{b}-\sqrt{3}D}{2\sqrt{3}L_\mathrm{FPZ}} w_\mathrm{c} + W_{x,\mathrm{Ec}} \tag{32}$$

2.8 Development of cover delamination

After $d_{\mathrm{f,max,u}} < d_{\mathrm{f,max}}$, the bulging of the concrete cover surface is primarily attributed to the uplifting movement of the concrete cover, i.e.,

$$d_{\mathrm{f,max}} = d_{\mathrm{cs}}(x) \tag{33}$$

As corrosion progresses, the bulging gradually increases and delamination of the concrete eventually takes place.

3. Finite element model

A nonlinear FE analysis was carried out with ATENA to verify the analytical model developed in Section 2. To examine the concrete cover delamination, three rebars were used in the FE model. The schematics and boundary conditions of the concrete samples is shown in Fig. 7 and the rebar diameter, cover thickness, rebar spacing and concrete properties (modeled by using the SBETA material model with an exponential tension softening curve) used in the simulation are provided in Table 1. It has been found that the failure modes of concrete covers caused by interior and corner rebars are different [18, 24, 33, 55, 56] due to mainly the difference in boundary conditions. As this study focuses on the cover delamination caused by the interior rebars, only the middle rebar and the concrete cover in the middle of the sample in Fig. 7 are examined.

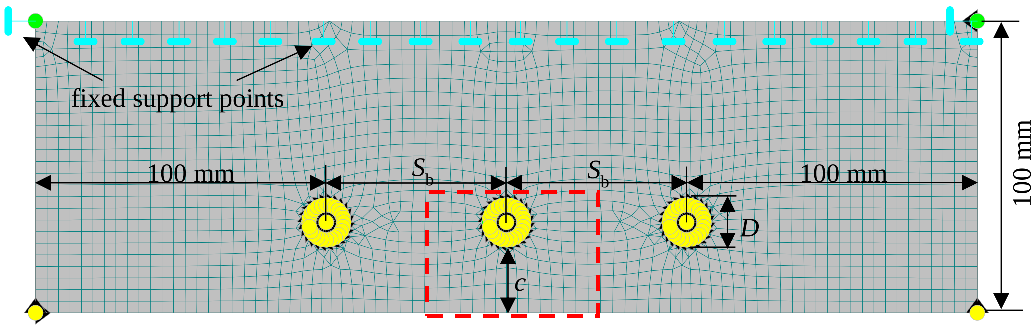

Fig. 7 Schematics and boundary conditions of concrete sample

Table 1 Rebar diameter, cover thickness, rebar spacing and concrete properties

Rebar diameter D (mm)	Cover thickness c (mm)	Rebar spacing S_b (mm)	Tensile strength of concrete f_t (MPa)	Young's modulus of concrete $E_{c,ef}$ (GPa)
12	25	1.5D+c=49.5	2.317	30.23
12	35	2D+c=62	3.678	39.27
12	45	2.5D+c=74.5	4.82	43.69

The cross section of each rebar is evenly divided into 24 segments as shown in Fig. 8. Rust expansion was modeled by using the thermal analogy method and the increase in the rebar radius due to the expansion of rust is calculated by using:

$$d_{\mathrm{f,max}} = \alpha_l \Delta T \, D/2 \tag{34}$$

where $d_{\mathrm{f,max}}$ is the increase in the rebar radius, α_l is the thermal expansion coefficient of steel which is 1.2×10^{-5} m/(m·K) and ΔT is the increase in temperature. In order for the rust to distribute in a crescent shape, the temperature assigned to each segment of the partially corroded rebar is linearly reduced with an increase in the distance from every part of the steel to the cover surface as shown in Fig. 8.

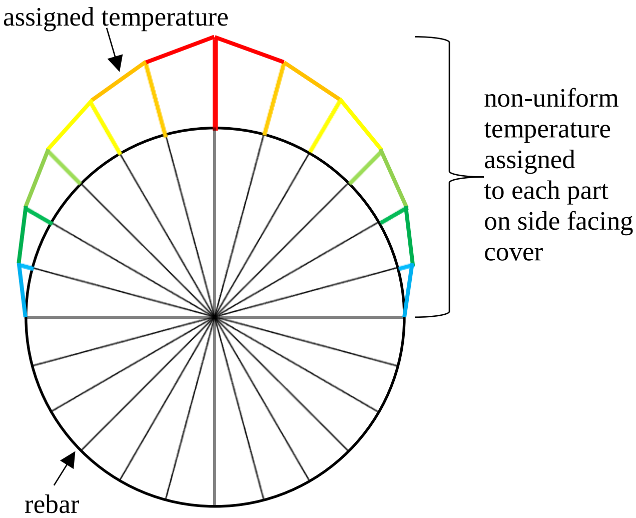

Fig. 8 Cross section and assigned temperature on segmented rebar

4. Verification and discussion

In this section, the process and progression of concrete cover delamination, $d_{f,max,Ec}$, $d_{cs}(x)$, $d_{f,max,u}$ and the relationship between $d_{f,max}$ and $d_{cs,A}$ obtained from the analytical and the FE models are compared for different S_b, f_t and c.

4.1 Process and progression of concrete cover delamination

The bulging of the concrete cover surface obtained by using ATENA for $d_{f,max}$ = 5 μm, 10 μm, 20 μm and 30 μm are shown in Fig. 9 in which the origin is in middle of the two rebars. The $d_{f,max,u}$ for the initiation of the concrete cover delamination is 18 μm. Therefore, $d_{f,max}$ = 5 μm and 10 μm in the partial cracking stage and $d_{f,max}$ = 20 μm and 30 μm in the stage in which delamination develops in the concrete cover. In the partial cracking stage, the bulging $d_{cs,A}$ is less than $d_{f,max}$, and $d_{cs}(x)$ decreases from Point A to Point M_1 (see Fig. 9a). In the stage where delamination develops in the concrete cover, the $d_{cs}(x)$ is almost the same and generally equal to $d_{f,max}$ as shown in Fig. 9b. The reason why the deformation at Point M is a little higher than that at Point A may be due to the effect of the neighboring corroded rebar. It can be concluded that the bulging of the concrete cover surface obtained by using ATENA perfectly supports the process and progression of the corrosion-induced delamination of the concrete cover as proposed in the analytical model.

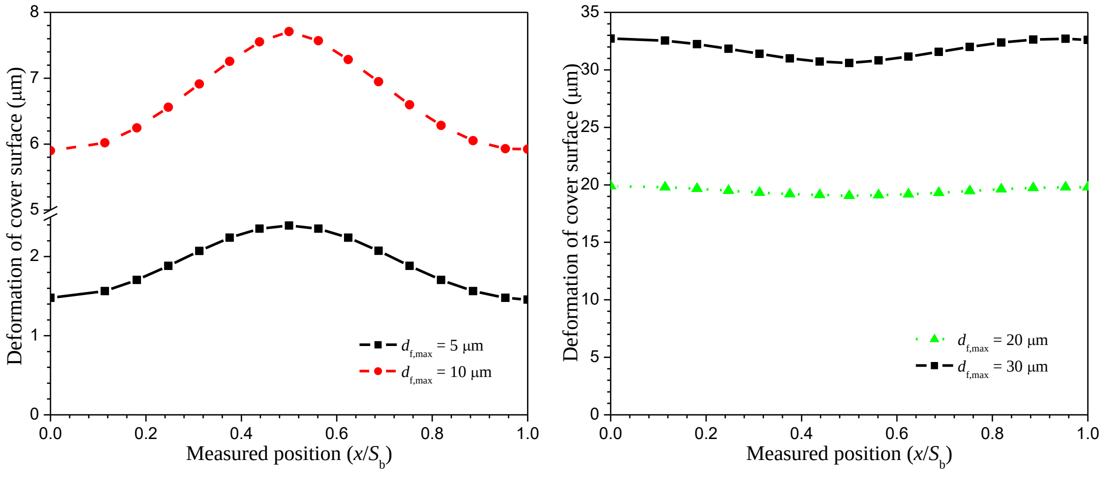

(a) (b)

Fig. 9 Bulging of cover surface $d_{cs}(x)$ obtained with ATENA for (a) net maximum thickness of rust $d_{f,max}$ = 5 μm and 10 μm and (b) $d_{f,max}$ = 20 μm and 30 μm (f_t = 2.317 MPa, $E_{c,ef}$ = 30.23 GPa, v = 0.2, D = 12 mm, β = 3, d_0 = 12.5 μm [1], c = 25, S_b = 62 mm, φ = 60°, L_{FPZ} = 130 mm [2, 3], w_c = 200 μm [10])

4.2 Net maximum thickness of corroded steel $d_{f,max,Ec}$

Fig. 10 is a comparison of the $d_{f,max,Ec}$ obtained from the proposed analytical and FE models for different f_t. It can be observed that the results obtained from the analytical model are in good agreement with those of the FE model. Moreover, $d_{f,max,Ec}$ increases with an increase in f_t. This is reasonable as a higher f_t will require a higher net maximum thickness of rust to initiate cracking in the concrete.

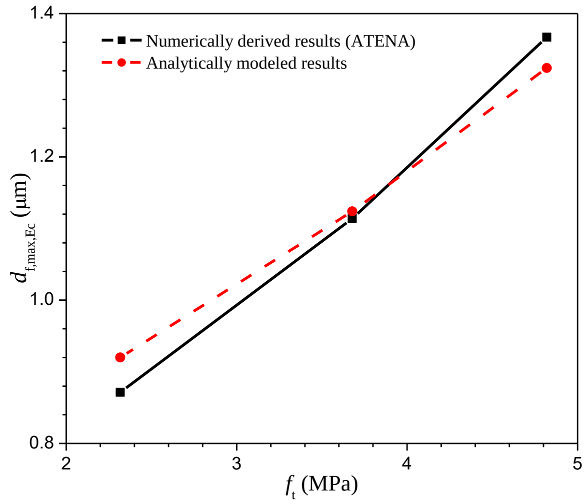

Fig. 10 Comparison of $d_{f,max,Ec}$ obtained from FE and analytical models (v = 0.2, D = 12 mm, β = 3, d_0 = 12.5 μm, c = 25, S_b = 62 mm, φ = 60°, L_{FPZ} = 130 mm, w_c = 200 μm)

4.3 Surface deformation along AC $d_{cs}(x)$

A comparison of the $d_{cs}(x)$ obtained from the analytical and the FE models are shown in Fig. 11 for different S_b, f_t and c. It can be observed that all of the results of the analytical model agree well with those of the FE model.

Figs. 11a-11c show the effects of S_b, f_t and c on the $d_{cs}(x)$ in the partial cracking stage when $d_{f,max}$ = 5 μm. It can be observed that for the same $d_{f,max}$, the $d_{cs}(x)$ decreases with an increase of S_b. This is because a wider S_b means a greater confinement effect of the concrete along HM. This is reasonable as a higher strength concrete with a thicker cover will inhibit the initiation of corrosion. However, it is interesting to find that f_t and c have almost no influence on $d_{cs}(x)$ for the same $d_{f,max}$.

The effects of S_b, f_t and c on $d_{cs}(x)$ on the development of delamination in the concrete cover when $d_{f,max}$ = 30 μm are shown in Figs. 11d and 11e. It can be observed that S_b, f_t and c have no effects on $d_{cs}(x)$ as $d_{cs}(x)$ is determined by $d_{f,max}$ in this stage.

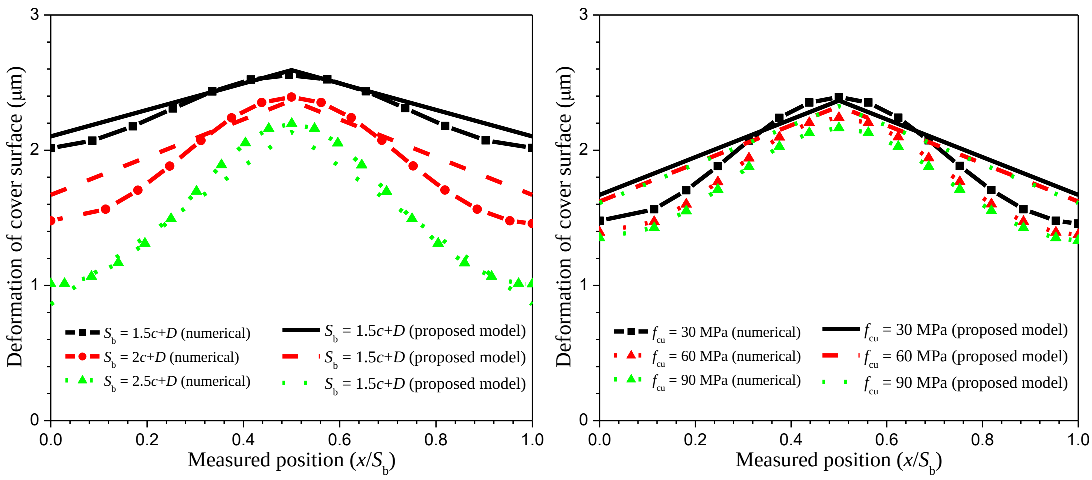

(a) (b)

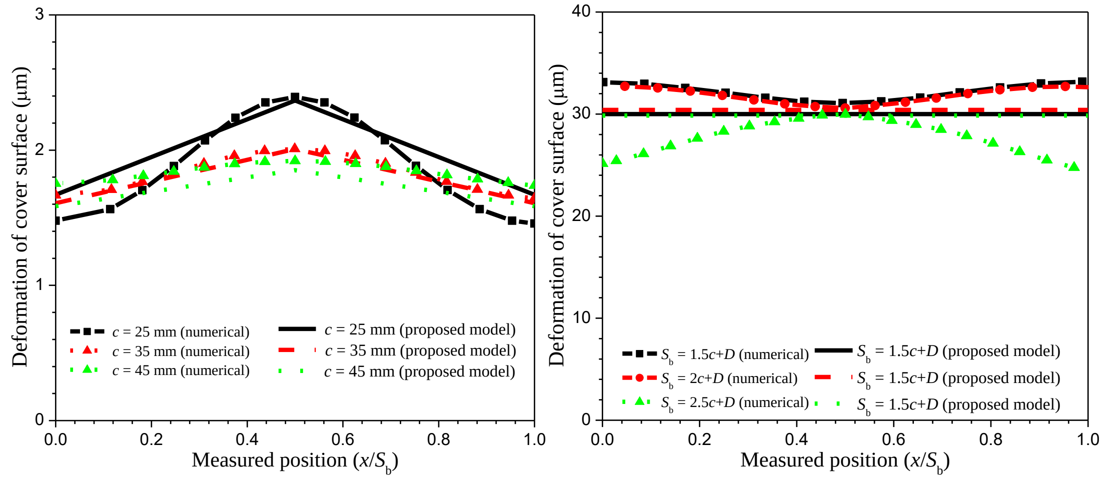

(c) (d)

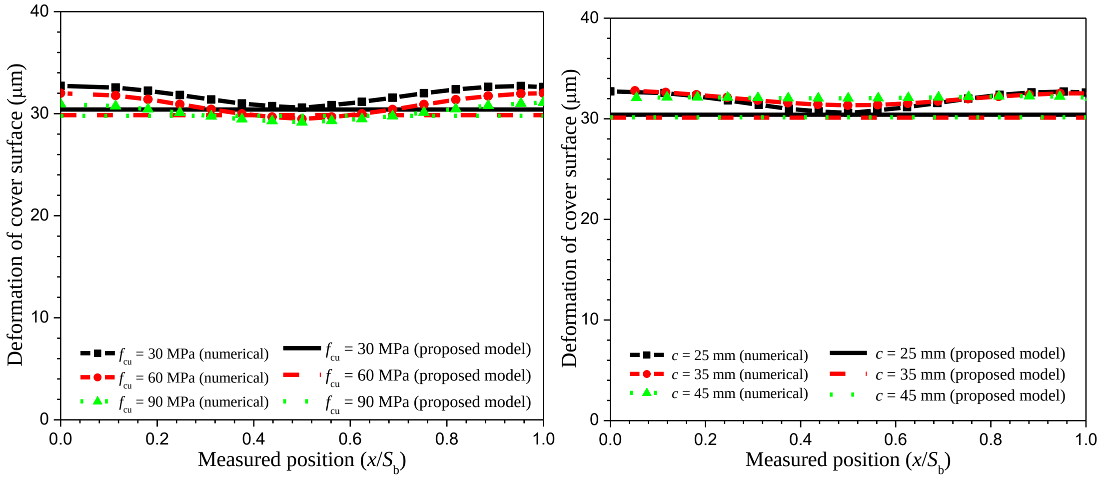

(e) (f)

Fig. 11 Comparison of $d_{cs}(x)$ obtained from analytical and FE models: effects of (a) rebar spacing (f_t = 2.317 MPa, $E_{c,ef}$ = 30.23 GPa, c = 25), (b) tensile strength of concrete (S_b = 62 mm, c = 25) and (c) cover thickness (f_t = 2.317 MPa, $E_{c,ef}$ = 30.23 GPa, S_b = 62 mm) in the partial cracking stage; effects of (d) rebar spacing, (e) tensile strength of concrete and (f) cover thickness in development of delamination in concrete cover (v = 0.2, D = 12 mm, β = 3, d_0 = 12.5 μm, φ = 60°, L_{FPZ} = 130 mm, w_c = 200 μm)

4.4 Net maximum thickness of rust $d_{f,max,u}$

Fig. 12 shows the $d_{f,max,u}$ obtained from the analytical and the FE models for different S_b, f_t and c. It can be observed that the analytically modeled results are in good agreement with the numerically derived results. Furthermore, $d_{f,max,u}$ increases with an increase in S_b while f_t and c have almost no effect on $d_{f,max,u}$. This is because when uplift begins to occur on the concrete cover, the concrete cover can be affected by S_b as shown in Eqs. (31) and (32), but f_t and c have almost no effect.

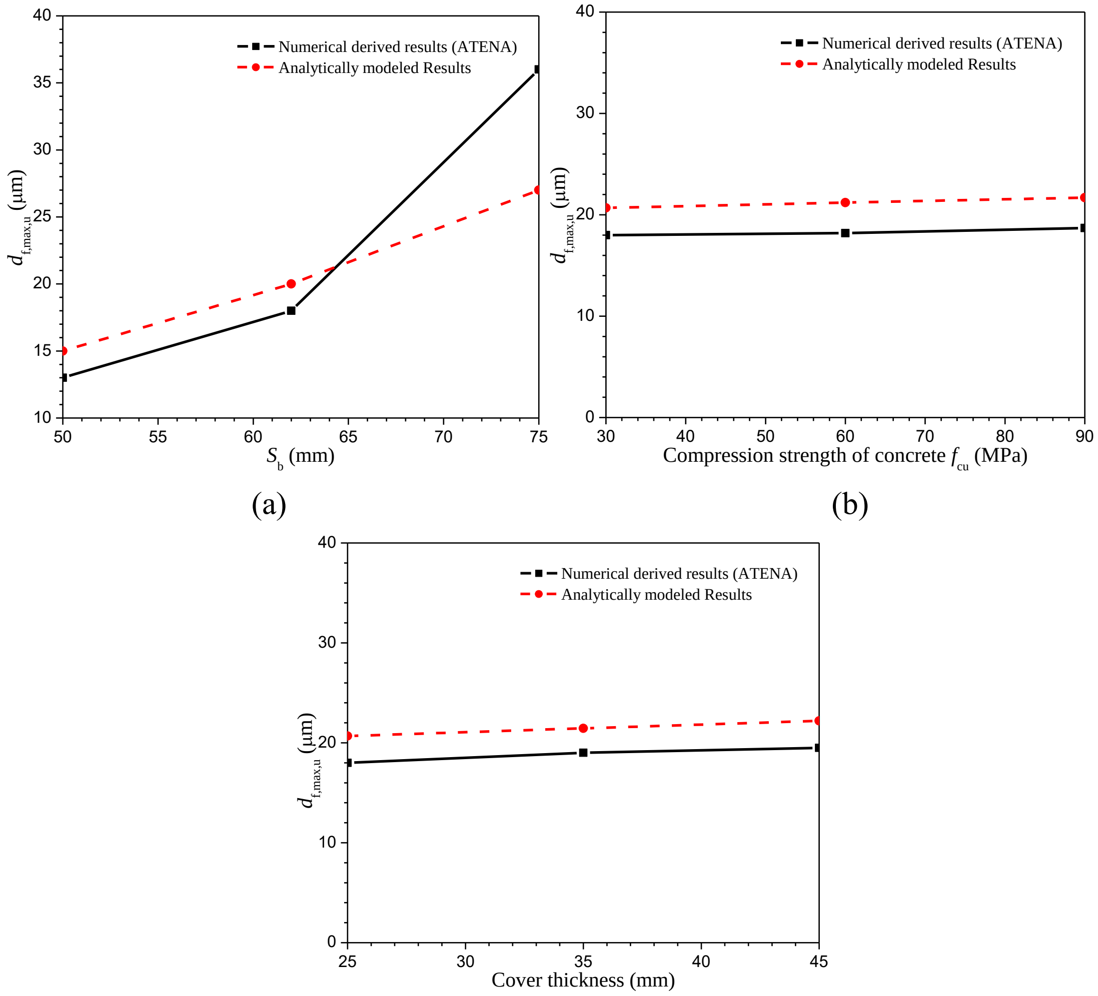

(a) (b)

(c)

Fig. 12 Comparison of $d_{f,max,u}$ obtained from analytical and FE models: effects of (a) rebar spacing (f_t = 2.317 MPa, $E_{c,ef}$ = 30.23 GPa, c = 25), (b) tensile strength of concrete (S_b = 62 mm, c = 25) and (c) cover thickness (f_t = 2.317 MPa, $E_{c,ef}$ = 30.23 GPa, v = 0.2, S_b = 62 mm) (D = 12 mm, β = 3, d_0 = 12.5 μm, φ = 60°, L_{FPZ} = 130 mm, w_c = 200 μm)

4.5 Relationship between $d_{f,max}$ and $d_{cs,A}$

Fig. 13 is a comparison of the relationship between $d_{f,max}$ and $d_{cs,A}$ which are obtained from the proposed analytical and FE models. It can be seen that all of the analytically modeled results agree well with the results obtained from the FE model.

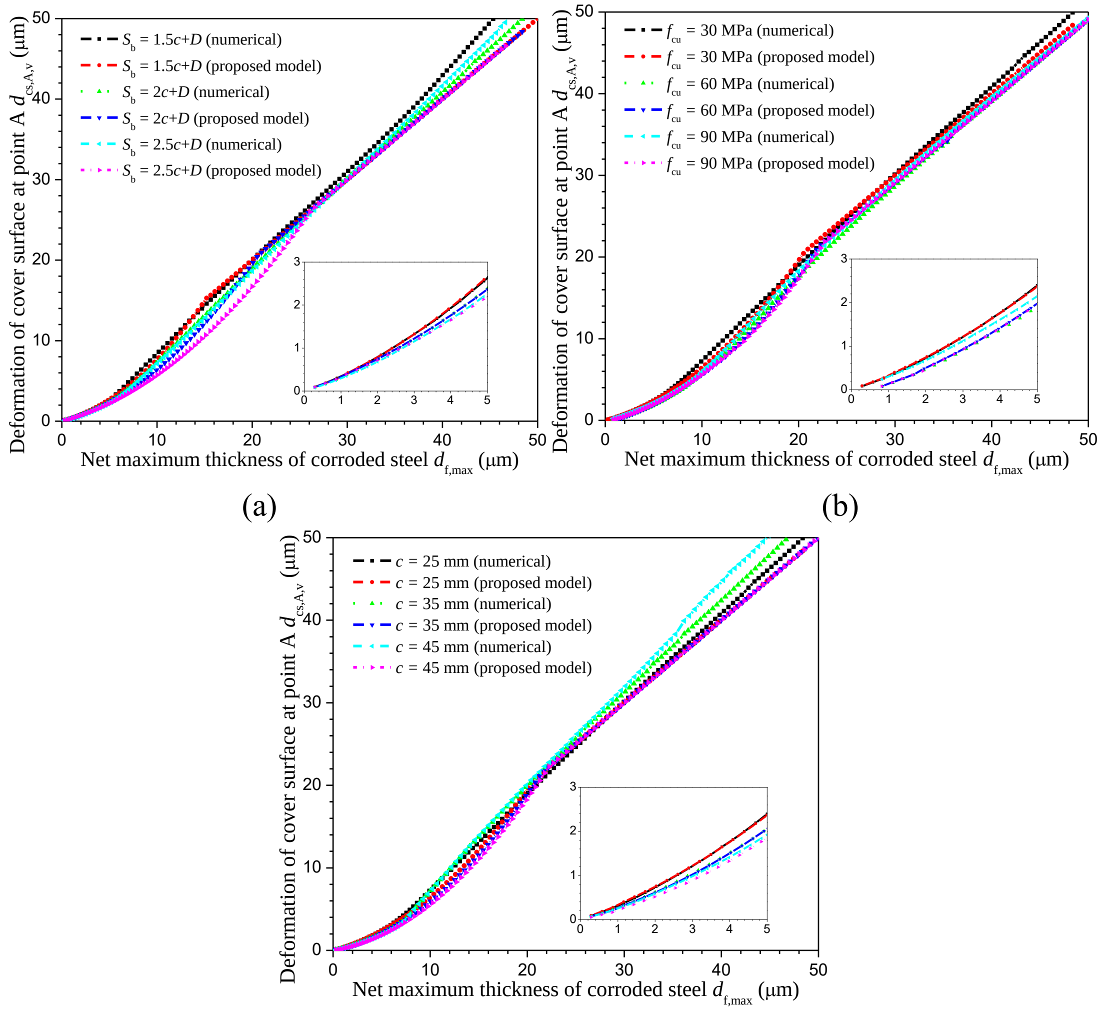

(c)

Fig. 13 Comparison of relationship between $d_{f,max}$ and $d_{cs,A}$ obtained from analytical and FE models: effects of (a) rebar spacing (f_t = 2.317 MPa, $E_{c,ef}$ = 30.23 GPa, c = 25), (b) tensile strength of concrete (S_b = 62 mm, c = 25) and (c) cover thickness (f_t = 2.317 MPa, $E_{c,ef}$ = 30.23 GPa, S_b = 62 mm) (ν = 0.2, D = 12 mm, β = 3, d_0 = 12.5 μm, φ = 60°, L_{FPZ} = 130 mm, w_c = 200 μm)

5. Conclusions

In this study, a novel analytical model is proposed to simulate the concrete cover delamination caused by multiple rebars that are closely spaced in RC structures by taking into consideration (1) the interaction of the neighboring corroded rebars, (2) the non-uniform distribution of rust around the steel/concrete interface, and (3) a flat concrete surface.

A nonlinear FE analysis has been carried out with ATENA to simulate the non-uniform expansion of rust by using the thermal analogy method. The analytical model has been verified through a comparison of the analytically modeled results with the numerically derived results.

The process and progression of the bulging of the concrete cover surface due to delamination are determined by using the analytical model. The progression of the concrete cover delamination can be examined as three stages: the elastic stage of the concrete, partial cracking stage and the stage in which there is development of delamination in the concrete cover.

In the partial cracking stage, the bulging of the concrete cover surface is reduced with an increase in rebar spacing. However, the tensile strength of concrete and cover thickness have almost no influence on the bulging of the concrete cover surface.

In the stage in which delamination develops in the concrete cover, it is found that the bulging is equal to the maximum thickness of the rust. Furthermore, the rebar spacing, tensile strength of the concrete and cover thickness have no effects on the bulging of the concrete cover surface.

This proposed model could be used to predict the amount of corrosion in rebars based on the measured amount of bulging of the concrete cover surface.

Acknowledgements

This research work is not linked to any specific grant from a public, commercial or non-profit funding agency.

References

[1] R.K.L. Su, Y. Zhang, A double-cylinder model incorporating confinement effects for the analysis of corrosion-caused cover cracking in reinforced concrete structures, Corrosion Science 99 (2015) 205-218.

[2] K. Otsuka, H. Date, Fracture process zone in concrete tension specimen, Engineering Fracture Mechanics 65(2) (2000) 111-131.

[3] S.Y. Alam, J. Saliba, A. Loukili, Fracture examination in concrete through combined digital image correlation and acoustic emission techniques, Construction and Building Materials 69 (2014) 232-242.

[4] Y. Liu, R. Weyers, Modeling the time-to-corrosion cracking in chloride contaminated reinforced concrete structures, ACI Materials Journal 95(6) (1998) 675-681.

[5] F. Chen, H. Baji, C.-Q. Li, A comparative study on factors affecting time to cover cracking as a service life indicator, Construction and Building Materials 163 (2018) 681-694.

[6] Y. Zhao, J. Yu, W. Jin, Damage analysis and cracking model of reinforced concrete structures with rebar corrosion, Corrosion Science 53(10) (2011) 3388-3397.

[7] A. Dasar, H. Hamada, Y. Sagawa, D. Yamamoto, Deterioration progress and performance reduction of 40-year-old reinforced concrete beams in natural corrosion

environments, Construction and Building Materials 149 (2017) 690-704.
[8] D. Li, R. Wei, F. Xing, L. Sui, Y. Zhou, W. Wang, Influence of non-uniform corrosion of steel bars on the seismic behavior of reinforced concrete columns, Construction and Building Materials 167 (2018) 20-32.
[9] H. Ye, C. Fu, N. Jin, X. Jin, Performance of reinforced concrete beams corroded under sustained service loads: A comparative study of two accelerated corrosion techniques, Construction and Building Materials 162 (2018) 286-297.
[10] H.H. Chen, R.K.L. Su, Tension softening curves of plain concrete, Construction and Building Materials 44 (2013) 440-451.
[11] C.Q. Li, S.T. Yang, Prediction of concrete crack width under combined reinforcement corrosion and applied load, Journal of Engineering Mechanics 137(11) (2011) 722-731.
[12] X. Xi, S. Yang, Time to surface cracking and crack width of reinforced concrete structures under corrosion of multiple rebars, Construction and Building Materials 155 (2017) 114-125.
[13] Y. Yuan, Y. Ji, Modeling corroded section configuration of steel bar in concrete structure, Construction and Building Materials 23(6) (2009) 2461-2466.
[14] W. Zhu, R. François, Y. Liu, Propagation of corrosion and corrosion patterns of bars embedded in RC beams stored in chloride environment for various periods, Construction and Building Materials 145 (2017) 147-156.
[15] Y. Zhao, B. Hu, J. Yu, W. Jin, Non-uniform distribution of rust layer around steel bar in concrete, Corrosion Science 53(12) (2011) 4300-4308.
[16] S. Muthulingam, B.N. Rao, Non-uniform corrosion states of rebar in concrete under chloride environment, Corrosion Science 93 (2015) 267-282.
[17] K.V. Subramaniam, M. Bi, Investigation of steel corrosion in cracked concrete: evaluation of macrocell and microcell rates using Tafel polarization response, Corrosion Science 52(8) (2010) 2725-2735.
[18] X. Zhu, G. Zi, A 2D mechano-chemical model for the simulation of reinforcement corrosion and concrete damage, Construction and Building Materials 137 (2017) 330-344.
[19] E. Chen, C.K.Y. Leung, Finite element modeling of concrete cover cracking due to non-uniform steel corrosion, Engineering Fracture Mechanics 134 (2015) 61-78.
[20] D. Qiao, H. Nakamura, Y. Yamamoto, T. Miura, Crack patterns of concrete with a single rebar subjected to non-uniform and localized corrosion, Construction and Building Materials 116 (2016) 366-377.
[21] B.S. Jang, B.H. Oh, Effects of non-uniform corrosion on the cracking and service life of reinforced concrete structures, Cement and Concrete Research 40(9) (2010) 1441-1450.

[22] J. Zhang, X. Ling, Z. Guan, Finite element modeling of concrete cover crack propagation due to non-uniform corrosion of reinforcement, Construction and Building Materials 132 (2017) 487-499.
[23] Y. Zhao, A.R. Karimi, H.S. Wong, B. Hu, N.R. Buenfeld, W. Jin, Comparison of uniform and non-uniform corrosion induced damage in reinforced concrete based on a Gaussian description of the corrosion layer, Corrosion Science 53(9) (2011) 2803-2814.
[24] X. Du, L. Jin, R. Zhang, Modeling the cracking of cover concrete due to non-uniform corrosion of reinforcement, Corrosion Science 89 (2014) 189-202.
[25] E. Chen, C.K.Y. Leung, A coupled diffusion-mechanical model with boundary element method to predict concrete cover cracking due to steel corrosion, Corrosion Science 126 (2017) 180-196.
[26] T. El Maaddawy, K. Soudki, A model for prediction of time from corrosion initiation to corrosion cracking, Cement and Concrete Composites 29(3) (2007) 168-175.
[27] C. Lu, W. Jin, R. Liu, Reinforcement corrosion-induced cover cracking and its time prediction for reinforced concrete structures, Corrosion Science 53(4) (2011) 1337-1347.
[28] X. Zhang, M. Li, L. Tang, S.A. Memon, G. Ma, F. Xing, H. Sun, Corrosion induced stress field and cracking time of reinforced concrete with initial defects: Analytical modeling and experimental investigation, Corrosion Science 120 (2017) 158-170.
[29] S. Caré, Q. Nguyen, K. Beddiar, Y. Berthaud, Times to cracking in reinforced mortar beams subjected to accelerated corrosion tests, Materials and Structures 43(1-2) (2010) 107-124.
[30] Z. Cui, A. Alipour, Concrete cover cracking and service life prediction of reinforced concrete structures in corrosive environments, Construction and Building Materials 159 (2018) 652-671.
[31] S. Guzmán, J.C. Gálvez, Modelling of concrete cover cracking due to non-uniform corrosion of reinforcing steel, Construction and Building Materials 155 (2017) 1063-1071.
[32] C. Fahy, S.J. Wheeler, D. Gallipoli, P. Grassl, Corrosion induced cracking modelled by a coupled transport-structural approach, Cement and Concrete Research 94(C) (2017) 24-35.
[33] X. Xi, S. Yang, C.-Q. Li, A non-uniform corrosion model and meso-scale fracture modelling of concrete, Cement and Concrete Research 108 (2018) 87-102.
[34] Q. Liu, R.K.L. Su, A displacement-based inverse analysis method to estimate in-situ Young's modulus of steel rust in reinforced concrete, Engineering Fracture

Mechanics 192 (2018) 114-128.

[35] A. Chen, Z. Pan, R. Ma, Mesoscopic simulation of steel rebar corrosion process in concrete and its damage to concrete cover, Structure and Infrastructure Engineering 13(4) (2017) 478-493.

[36] W. Dong, Y. Murakami, H. Oshita, S. Suzuki, T. Tsutsumi, Influence of both stirrup spacing and anchorage performance on residual strength of corroded RC beams, Journal of Advanced Concrete Technology 9(3) (2011) 261-275.

[37] A. Jamali, U. Angst, B. Adey, B. Elsener, Modeling of corrosion-induced concrete cover cracking: A critical analysis, Construction and Building Materials 42 (2013) 225-237.

[38] C.Q. Li, J.J. Zheng, W. Lawanwisut, R.E. Melchers, Concrete delamination caused by steel reinforcement corrosion, Journal of Materials in Civil Engineering 19(7) (2007) 591-600.

[39] G. Sterritt, Probabilistic techniques for lifetime management of reinforced concrete highway bridges, Imperial College London, 2000.

[40] Y.G. Du, A.H.C. Chan, L.A. Clark, X.T. Wang, F. Gurkalo, S. Bartos, Finite element analysis of cracking and delamination of concrete beam due to steel corrosion, Engineering Structures 56(C) (2013) 8-21.

[41] I. Balafas, C.J. Burgoyne, Environmental effects on cover cracking due to corrosion, Cement and Concrete Research 40(9) (2010) 1429-1440.

[42] F.J. Molina, C. Alonso, C. Andrade, Cover cracking as a function of rebar corrosion: Part 2—Numerical model, Materials and Structures 26(9) (1993) 532-548.

[43] Y. Zhao, Y. Wu, W. Jin, Distribution of millscale on corroded steel bars and penetration of steel corrosion products in concrete, Corrosion Science 66 (2013) 160-168.

[44] Y. Zhao, H. Ren, H. Dai, W. Jin, Composition and expansion coefficient of rust based on X-ray diffraction and thermal analysis, Corrosion Science 53(5) (2011) 1646-1658.

[45] B. Sanz, J. Planas, J.M. Sancho, A method to determine the constitutive parameters of oxide in accelerated corrosion tests of reinforced concrete specimens, Cement and Concrete Research 101 (2017) 68-81.

[46] U. Angst, M. Geiker, A. Michel, C. Gehlen, H. Wong, O. Isgor, B. Elsener, C. Hansson, R. François, K. Hornbostel, R. Polder, M. Alonso, M. Sanchez, M. Correia, M. Criado, A. Sagüés, N. Buenfeld, The steel–concrete interface, Materials and Structures 50(2) (2017) 1-24.

[47] D.V. Val, L. Chernin, M.G. Stewart, Experimental and numerical investigation of corrosion-induced cover cracking in reinforced concrete structures, Journal of Structural Engineering 135(4) (2009) 376-385.

[48] Y. Zhao, J. Dong, Y. Wu, W. Jin, Corrosion-induced concrete cracking model considering corrosion product-filled paste at the concrete/steel interface, Construction and Building Materials 116 (2016) 273-280.
[49] L. Chernin, D. Val, K. Volokh, Analytical modelling of concrete cover cracking caused by corrosion of reinforcement, Materials and Structures 43(4) (2010) 543-556.
[50] K. Kim, S. Jang, B. Jang, B. Oh, Modeling mechanical behavior of reinforced concrete due to corrosion of steel bar, ACI Materials Journal 107(2) (2010) 106-113.
[51] H.S. Wong, Y.X. Zhao, A.R. Karimi, N.R. Buenfeld, W.L. Jin, On the penetration of corrosion products from reinforcing steel into concrete due to chloride-induced corrosion, Corrosion Science 52(7) (2010) 2469-2480.
[52] Y. Zhao, J. Yu, Y. Wu, W. Jin, Critical thickness of rust layer at inner and out surface cracking of concrete cover in reinforced concrete structures, Corrosion Science 59 (2012) 316-323.
[53] A.C. Ugural, S.K. Fenster, Advanced strength and applied elasticity, Elsevier Science Publishing Company Inc., The Netherlands, 1977.
[54] S. Care, Mechanical properties of the rust layer induced by impressed current method in reinforced mortar, Cement and Concrete Research 38(8-9) (2008) 1079-1091.
[55] J. Ožbolt, F. Oršanić, G. Balabanić, M. Kušter, Modeling damage in concrete caused by corrosion of reinforcement: coupled 3D FE model, International Journal of Fracture 178(1) (2012) 233-244.
[56] P.J. Sánchez, A.E. Huespe, J. Oliver, S. Toro, Mesoscopic model to simulate the mechanical behavior of reinforced concrete members affected by corrosion, International Journal of Solids and Structures 47(5) (2010) 559-570.